

Molecular interaction volume model of mixing enthalpy for molten salt system: An integrated calorimetry-model case study of LaCl_3 -(LiCl-KCl)

Vitaliy G. Goncharov^{1,2}, William Smith¹, Jiahong Li¹, Jeffrey A. Eakin¹, Erik D. Reinhart¹, James Boncella¹, Luke D. Gibson,³ Vyacheslav S. Bryantsev,⁴ Rushi Gong⁵, Shun-Li Shang⁵, Zi-Kui Liu⁵, Hongwu Xu^{6,7}, Aurora Clark,^{1,8,*} Xiaofeng Guo^{1,2,*}

¹ *Department of Chemistry, Washington State University, Pullman, Washington, 99164, United States*

² *Materials Science and Engineering Program, Washington State University, Pullman, Washington 99164, United States*

³ *Computational Sciences and Engineering Division, Oak Ridge National Laboratory, P.O. Box 2008, Oak Ridge, TN 37831, United States*

⁴ *Chemical Science Division, Oak Ridge National Laboratory, P.O. Box 2008, Oak Ridge, TN 37831, United States*

⁵ *Department of Materials Science and Engineering, Pennsylvania State University, University Park, PA 16802, United States*

⁶ *Earth and Environmental Sciences Division, Los Alamos National Laboratory, Los Alamos, New Mexico, NM 87545, United States*

⁷ *Arizona State University, Tempe, AZ, United States*

⁸ *Department of Chemistry, The University of Utah, Salt Lake City, Utah 84112, United States*

*E-mails: aurora.clark@utah.edu, x.guo@wsu.edu

Abstract: Calorimetric determination of enthalpies of mixing (ΔH_{mix}) of multicomponent molten salts often employs empirical models that lack parameters with clear physical interpretation (e.g., coordination numbers, molar volumes, and pair potentials). Although such physics informed models are not always needed, a thermodynamic understanding of the relationships between excess energies of mixing and local to intermediate solvation structures is particularly important for pyrochemical separation, as is the case for lanthanides (Ln), which are common neutron poisons and critical industrial elements found in spent nuclear fuels. Here we implement the molecular interaction volume model (MIVM) to synthesize information from experimentally measured ΔH_{mix} (using high temperature melt drop calorimetry) and the distribution of solvation structures from *ab initio* molecular dynamics (AIMD) simulations. This was demonstrated by a case study of molten salt system consisted of LaCl_3 mixing with a eutectic LiCl-KCl (58mol% – 42mol%) at 873 K and 1133 K. The parameters modelled from MIVM were used to extrapolate excess Gibbs energy (ΔG_{mix}), and compositional dependence of La^{3+} activity in the LaCl_3 -(LiCl-KCl) system. In contrast, by AIMD or polarizable ion model (PIM) simulations, a significant deviation regarding the predicted ΔH_{mix} was seen if computed directly from the molecular dynamic trajectories. The integrated experimental and simulation data within the MIVM formalism are generalizable to a wide variety of molten salts and demonstrate a significant improvement over currently employed methods to study molten salts for nuclear and separations sciences.

Key Words: Enthalpy of mixing; molecular interaction volume model; calorimetry; *ab initio* molecular dynamics; solvation structure; lanthanides

1 Introduction

Molten salt pyrochemical processing is an effective separation technique for actinides (An) and lanthanides (Ln), which is often a challenge due to their chemical similarity.¹⁻⁴ Its implementation and optimization require fundamental thermodynamic understanding of salt properties. Of particular interest is the excess Gibbs energy, which derives from the solvation structure of the mixed components. The dominating term enthalpy of mixing (ΔH_{mix}) can be experimentally accessed by high temperature drop calorimetry,⁵⁻¹² and is also effectively studied by first-principle calculations, such as *ab-initio* molecular dynamics (AIMD) based on density functional theory (DFT), providing information on metal chemistry and speciation (e.g., coordination number and interatomic pair potential).¹³⁻¹⁸ Although various thermodynamic models are available to couple thermochemical data (e.g., ΔH_{mix}) and phase equilibrium data based on the Calculation of Phase Diagrams (CALPHAD) method,^{19,20} most of these models include fitting parameters to be optimized, rather than being directly obtained from experiments or simulations. Given the potential of ΔH_{mix} to link solvation structure from the atomic scale to thermochemical properties at the macroscopic level, a model with chemically intuitive parameters would have unique advantages for developing the fundamental understanding needed for rational design of salt composition and operational conditions to tailor separation. In this work, we showcase an integration of the physically interpretable model (molecular interaction volume model, MIVM^{21,22}), with experimental calorimetry and computational efforts (AIMD and the polarizable ion model (PIM) simulations²³⁻²⁵), and its application to reveal the structure-energetic landscape of a molten chloride salt system.

The pseudo-binary LaCl_3 -(LiCl-KCl) molten salt has been studied, where (LiCl-KCl) is in its eutectic composition (~ 58 mol% LiCl and ~42 mol% KCl) with a melting temperature of 773 K.²⁶ When molten, eutectic LiCl-KCl can provide anodic dissolution of metallic spent nuclear fuel (SNF) during pyroprocessing, with An and Ln of interest recovered on the cathode surface via electrochemical deposition through applications of appropriate reductive potentials.²⁷ Molten salt pyrochemical processing offers a promising solution to separate metallic SNF from an open fuel cycle (used by majority of countries with active nuclear energy programs)^{28,29}, and to cycle up to 96% of critical metals, such as U back to fresh fuels³⁰⁻³², as well as a number of fission products that have industrial significance. In this work, LaCl_3 was selected as a constituent salt to be mixed with eutectic LiCl-KCl because they constitute ~1/3 of the fission products in SNF¹ and they present as a major challenge.^{27,33,34} Uncertainty of the speciation and associated stability within the melt has deleterious effects on the efficiency and effectiveness of An-Ln separation.³⁵ On the other hand, extraction of Ln from SNF provides an alternative source for critical metals rather than from rare-earth element (REE) deposits ore which often only enrich light REE and are commonly

accompanied with high Th or U contents.³⁶ With high demands of separating Ln from SNF,^{37–40} it is key to understand speciation and thermodynamics of La (as a surrogate for Ln in general) in eutectic LiCl-KCl.

Although prior calorimetric investigations of ΔH_{mix} of molten Ln chlorides with alkali/alkaline-earth metal chlorides have been reported,^{41–47} the origins of the thermodynamic non-ideality (which may be due to the formation of complexes, oligomers, or metal-chloride networks induced by the “guest” metal salt component) are not well understood.^{48,49} The correlation between solvation structure and energetics are not straightforward and rely heavily upon parameterized empirical models; the most commonly used are the associated solution model (ASM)^{41–47} and the surrounded ion model (SIM)⁴. ASM assumes that the irregularity of mixing behavior may be expressed as a linear combination of regular mixing interactions ($\Delta_{\text{mix}}H^{\text{REG}}$) and locally ordered “associates” ($\Delta_{\text{mix}}H^{\text{ASSOC}}$).⁵⁰ From ASM, one can further derive the interaction parameter (λ) by $\lambda = \Delta H_{\text{mix}}/x \cdot (1-x)$ with x being the primary mixed chloride (e.g., LnCl_3)⁵⁰. λ can further be deconvoluted into a linear combination of coulombic and polarization interactions and the formation enthalpy of the associates. In assuming small deviations from regular solution behavior and ignoring solvation beyond first cation-anion coordination, ASM is quantitatively inadequate to describe some spectroscopic and computational results.⁵¹ Alternatively, the SIM model is largely configuration based and primarily considers the charge of the mixing ions, with charge unsymmetric cations substitution yielding vacancies on the corresponding sublattices.⁵² It allows for fitting of multicomponent salt systems, although the number of charge asymmetries is limited (i.e., trivalent + monovalent salts). SIM also does not reflect directly solvation structure,^{51,53} and is subject to overfitting. These models demonstrate that there is significant opportunity to develop models with quantitative correlation of ΔH_{mix} to solvation structure and chemistry. On the other side with the computational efforts, a completely different approach entails the computation of ΔH_{mix} directly from the molecular dynamics (MD) trajectory obtained using either an empirical model (such as PIM) or DFT, typically employed at the generalized gradient approximation (GGA) for the exchange-correlation energy. While this approach does not introduce any additional empirical parameters beyond those used to describe the underlying computational method, it was noted that such ‘direct methods’ lack sufficient accuracy and often overpredict the magnitude of ΔH_{mix} for molten salts systems containing multivalent metal ions (e.g., Be^{2+} , U^{3+} , U^{4+} , Th^{4+} , etc.)^{54–56}.

Toward this end, we studied the mixing of LaCl_3 with 58mol% LiCl – 42mol% KCl eutectic melt using experimental calorimetry, together with AIMD and PIM modeling of ΔH_{mix} using the ‘direct method’, followed by implementing a modified MIVM for integrated data analysis. Within the calorimetry, a measurement temperature of 873 K for the low La content salts was chosen due to similar condition used in pyroprocessing²⁷, while a higher temperature of 1133 K was used to melt and access the high La content salts and to perform AIMD and PIM simulations across the whole LaCl_3 -(LiCl-KCl) composition range.

An additional set of AIMD simulations was conducted at 1200 K, from which we obtained the radius distribution functions (RDF) and potential of mean force (PMF) of various metals, as well as the distribution of metal coordination number (CN) as a function of La content. The combined results, including enthalpies of mixing and solvation structures, were integrated to a modified MIVM mixing model that uses physically-based parameters that are either experimentally measurable and/or computationally available. Previously, MIVM has been used to explore the thermodynamics of mixing of binary, ternary, and high-order alloys.^{57,58} With modified MIVM in this work, we also demonstrated the use of MIVM for the first time on the molten salt system. The parameters used by the MIVM are all physical and include the coordination number, pair potential, and molar volume, all of which can be readily determined by computation or experiment,^{21,22,57} and thus will be very useful to be deployed more widely for thermodynamic studies in the molten salt community.

2 Methods

2.1 MIVM and its extension to model mixing enthalpy of molten salts

MIVM was originally formulated by Tao²² to describe the excess thermodynamic properties of multi-component liquid systems based on non-random migrating local compositions (molecular cells) formed by the interactions of mixed components. The original model (described in SI section 1 and **Figure S1**) has not been implemented in a multicomponent molten salt system. We applied a pseudo binary formulation of MIVM with a modified definition of coordination number to the mixing of LaCl₃ in eutectic LiCl-KCl, described by equation 1; here the component 1 is LaCl₃ and the component 2 is eutectic LiCl-KCl:

$$\frac{\Delta H_m^M}{RT} = \frac{1}{2} \left\{ \sum_{i=1}^2 Z_i x_i \times \left[\left(\frac{\sum_{j=1}^2 x_j B_{ji} \ln B_{ji}}{\sum_{j=1}^C x_j B_{ji}} \right)^2 - \left(\frac{\sum_{j=1}^2 (1 + \ln B_{ji}) x_j B_{ji} \ln B_{ji}}{\sum_{j=1}^C x_j B_{ji}} \right) \right] \right\} - \sum_{i=1}^2 x_i \left(\frac{\sum_{j=1}^2 x_j V_{mj} B_{ji} \ln B_{ji}}{\sum_{j=1}^2 x_j V_{mj} B_{ji}} \right) \quad (1)$$

where R is the gas constant (kJ/mol·K), T is the temperature (K), Z_i is the liquidus first shell coordination number of component i , V_{mj} is the liquidus molar volume of component j (cm³/mol), B_{ij} and B_{ji} are the pair potential parameters of the $i-j$ pairs defined as

$$B_{ij} = e^{-(\varepsilon_{ij}-\varepsilon_{jj})/RT}, \quad B_{ji} = e^{-(\varepsilon_{ji}-\varepsilon_{ii})/RT} \quad (2)$$

where ε_{ii} , ε_{jj} , and ε_{ij} (kJ/mol) refer to the potential energies of the $i-i$, $j-j$, and $i-j$ pairs, respectively.²²

In *equation 1*, Z_1 corresponds to the first cation shell CN of La^{3+} (La – La) in molten LaCl_3 , Z_2 corresponds to the averaged first cation shell CN of $\text{Li}^+:\text{K}^+$ in eutectic LiCl-KCl (0.58Li-K + 0.42K-Li). V_{m1} and V_{m2} correspond to the liquidus molar volumes of LaCl_3 and eutectic LiCl-KCl , respectively.²¹ The potential energies²² of the 1 – 1, 2 – 2, and 1 – 2 components pairs are likewise defined to correspond to the pair potentials of La–Cl–La (ϵ_{11}), Li:K–Cl–Li:K (ϵ_{22}), and La–Cl–Li:K (ϵ_{12}), respectively. Pair potential parameters, B_{12} and B_{21} , can then be obtained using *equation 2*.²¹

2.1 Calorimetry methods

2.1.1 Differential Drop Calorimetric (DDC) Method

An argon sealed ampule of ultra-dry LaCl_3 was transferred to and opened within a glovebox ($\text{O}_2 < 1$ ppm, $\text{H}_2\text{O} < 0.5$ ppm). LaCl_3 beads were then subsequently ground into a fine powder and pressed into ~20 mg pellets using a hand die. The pellets were then loaded within into an annealed 3D printed airtight dropper,⁵⁹ which was used to transfer the sample to the calorimeter. All the samples' preparations, loading and storage was done within the glovebox. The LaCl_3 pellets were then dropped from room temperature into the calorimetric chamber (ambient exposure of < 1 s) which contained a nickel crucible with the molten LiCl-KCl eutectic (~200 mg) at 873 K in a steady argon environment. Upon dissolution and mixing of LaCl_3 within the LiCl-KCl eutectic, continuous drop enthalpy (ΔH_{cd}) was obtained. The resulting ΔH_{cd} values were then deconvoluted using thermochemical cycles in **Table S1** yielding differential (or incremental) enthalpy of mixing ($dH_{\text{i,mix}}$) which denotes the changes in the heat of mixing corresponding to changes in La concentrations within the melt. LaCl_3 samples were dropped into the LiCl-KCl eutectic at periodic intervals (~1.25 hrs.) changing the mol% of La within the melt, thus generating $dH_{\text{i,mix}}$ values across the liquidus range of the $\text{LaCl}_3 - \text{LiCl-KCl}$ system at 873 K. The $dH_{\text{i,mix}}$ values were then cumulatively summed to obtain molar enthalpies of mixing (ΔH_{mix}) (**Table S1**), corresponding to the overall La concentration introduced into the eutectic LiCl-KCl melt. Validity of this method was evaluated based on the consistency of the ΔH_{mix} obtained from four independent trials reported in **Table S2**, with a curve presented in **Figure 1**.

2.1.2 Integral Drop Calorimetric (IDC) Method

LaCl_3 and LiCl-KCl powders were mixed in specific $\text{LaCl}_3 - \text{LiCl:KCl}$ ratios and homogenized using an agate pestle and mortar yielding 5 physical mixtures with LaCl_3 concentrations corresponding to 1.77, 5.09, 7.06, and 19.26 mol% LaCl_3 measured at 873 K. Additionally, 4 additional mixtures were prepared with

LaCl₃ concentrations corresponding to 28.68, 43.64, 68.95, and 82.36 mol% LaCl₃ and measured at 1133 K. Samples from the corresponding physical mixtures were then pressed into ~10 mg pellets using a hand dye and loaded into annealed 3D printed airtight droppers.⁶⁰ This approach is similar to literature work.^{61,62} The physical mixtures were then dropped from room temperature into the calorimetric chamber which contained empty nickel crucibles at either 873 K or 1133 K in a stable argon environment (~5 ml/min flow). Upon introduction of the physical mixtures into the calorimetric chamber the pellets underwent the following thermal reactions within the crucibles: *i*) melting of the eutectic; *ii*) dissolution of LaCl₃ within the eutectic; and *iii*) mixing of the LaCl₃ – LiCl-KCl systems. Upon completion of these reactions, the integral heat effect, termed the drop enthalpy of physical mixtures (ΔH_{pd}), was obtained. The resulting ΔH_{pd} values were then used in a corresponding thermochemical cycle (**Tables S3 and S4** for reactions at 873 and 1133 K, respectively) to calculate the molar ΔH_{mix} at a given physical mixture La content (**Table S5**). At least 3 consecutive measurements were made for a given physical mixture ratio, resulting in ΔH_{mix} values with experimentally bound uncertainties (**Table S5**). Data for the 873 and 1133 K trails are plotted as dark grey solid squares and solid diamonds in **Figure 1**, respectively, with two standard deviations serving as uncertainty bounds.

2.2 Computational methods

The CP2K package^{63,64} version 9.1 using the Quickstep module was employed for Born-Oppenheimer density functional theory molecular dynamics simulations. The small box size of the simulations meant that small fluctuations in the cell dimensions result in large density changes, therefore experimental densities were used for the construction of the simulations. The pure salt densities were determined using the linear temperature dependent density formula:

$$\rho = a - bT \quad (3)$$

where the a and b parameters for the LiCl, KCl, and LaCl₃ came from the molten salt database by Janz.⁶⁵ The ideal mixing model developed at Idaho National Laboratory (Eq. 4) was implemented to determine the density of the molten salt mixtures.⁶⁶ Where the density, ρ , is given by the summation of the individual weight fractions and densities, w_i and ρ_i , respectively.

$$\frac{1}{\rho_{salt,calc}} = \sum \frac{w_i}{\rho_i} \quad (4)$$

The simulation boxes were generated using PACKMOL,⁶⁷ the dimensions for the boxes ranged from (14.757 × 14.757 × 14.757 Å) to (20.45 × 20.45 × 20.45 Å), detailed information for the composition of

each simulation can be found in the SI. The equilibrium procedure was executed in the *NVT* ensemble using a Nosé thermostat at 1200 K, higher than the reported melting point for this range of La concentration in a LiCl-KCl eutectic⁶⁸. Geodecker, Teter, and Hutter (GTH) pseudopotentials with the Perdew, Burke, and Ernzerhof (PBE) exchange correlation function with D3 dispersion corrections were applied to all ions with accompanying DZVP-MOLOPT basis set for all ions.^{69–73} It is well documented that the generalized gradient approximation functions in DFT poorly describe systems with strongly correlated *d*- and *f*-elements. This was resolved through the use of a Hubbard-like term implemented via DFT+*U* with a U_{eff} value of 4 eV.⁷⁴ All simulations were run in the *NVT* ensemble with a time step of 1 fs for a total of 150 ps with the first third discarded prior to analysis. The potential of mean force (PMF) was determined by the radial distribution function using $PMF(x) = -k_B T \ln[P(x)]$, where the probability distribution $P(x)$ comes from the calculated RDF (shown in SI section 3, **Tables S7 and S8, Figures S2~S5**). Furthermore, additional computational detail for setting up PIM and AIMD simulations to directly compute the ΔH_{mix} are given in the SI section 4.

3 Results and Discussion

3.1 Computations of mixing enthalpy of $LaCl_3$ in eutectic LiCl – KCl from PIM and AIMD

The mixing enthalpies of molten salts can be computed directly from MD trajectories generated using the isothermal–isobaric ensemble (*NPT*) by averaging the normalized (per one molecular unit) potential energies across the composition range after subtracting the normalized potential energies of the end members, as follows:

$$\Delta H_{mix} = U_{AB} + (PV)_{AB} - x_A[U_A + (PV)_A] - x_B[U_B + (PV)_B], \quad (5)$$

where U , P , and V denote the internal energy, the system pressure, and system volume, respectively. Subscripts A and B correspond to the two pure component systems (i.e., eutectic LiCl-KCl and $LaCl_3$), while AB denotes mixtures with associated mole fractions, x_A and x_B . At conditions close to the atmospheric pressure, the PV term is small and can be omitted. For example, in our PIM *NPT* ($P = 1$ bar) simulations, the PV contribution to ΔH_{mix} is less than 0.02 kJ/mol. Consistent with the previous studies of molten salts containing multivalent cations,^{54–56} the PIM model reproduces the overall shape of ΔH_{mix} as a function of composition, but significantly overestimates the magnitude of ΔH_{mix} , by almost 100% at the most negative ΔH_{mix} value (**Figure 1**). We note that the PIM model²³ for $LaCl_3$ was fitted to reproduce experimental liquid density and structure functions from the scattering experiments and was not specifically trained to yield accurate thermodynamic parameters for the interaction of the individual salt’s components with its

environment. The absolute error in ΔH_{mix} produced by the PIM model is < 6 kJ/mol, which is in the range of accuracy expected from such a model. This emphasizes the grand challenge of the computational methods to achieve ‘chemical accuracy’ of ~ 4 kJ/mol or better in predicting reaction thermochemistry and, as such, provide a more accurate description of chemical potentials and phase diagrams.

The AIMD simulations using the PBE-D3 density functional for the same compositions were attempted to directly reproduce ΔH_{mix} . In this case, however, simulations were carried out in the canonical (NVT) ensemble, which are easier to converge than those in the NPT ensemble given limited AIMD sampling. A series of NVT simulations for different volumes were conducted to estimate the equilibrium density for each composition at the pressure near 1 bar (see **Figure S7**). In comparison to the experimental densities observed for the pure components, the PBE-D3 density functional underestimates the density of liquid LaCl_3 at $T = 1133$ K by 9.2%, yet provides an accurate density estimation for the LiCl-KCl eutectic mixture. The PIM and PBE-D3 densities deviate more as the mole fraction of LaCl_3 increases, with the PIM model accurately reproducing the density of liquid LaCl_3 . In this respect, the deficiency of DFT is likely related to underestimation of the interaction of LaCl_3 with its environment, which is consistent with previous observations⁵¹ that DFT-based AIMD simulations yielded smaller La-Cl CN and reduced first RDFs peaks for the La-Cl and La-La pairs compared to the PIM model. Mixing enthalpies using the AIMD NVT trajectories were computed on the cells with the smallest pressure magnitudes. The uncertainty in the ΔH_{mix} due to the average pressure deviating from 1 bar was estimated to be below 0.6 kJ/mol (**Figure S8**). In line with the PIM simulations, the magnitude of ΔH_{mix} from the AIMD simulations is significantly overestimated (more than twice) compared to the experimental values (**Figure 1**). In general, GGA DFT-based AIMD simulations are not expected to achieve a desirable level of ‘chemical accuracy’ for a diverse set of systems, especially for those containing f-block elements, where the self-interaction error of DFT becomes very prominent.⁷⁵ It remains to be seen if hybrid DFT methods can significantly reduce the error in ΔH_{mix} , or resorting to more accurate methods, such as Random Phase Approximation (RPA), coupled cluster, and/or quantum Monte Carlo would be necessary to bring the error down to the level expected from CALPHAD modeling. Another promising option is the use of machine learning (ML) force field developments for testing these more advanced quantum mechanical methods for predicting thermodynamic properties of molten salts.

3.2 Application of MIVM to the mixing enthalpy of LaCl_3 in eutectic $\text{LiCl} - \text{KCl}$

Table 1 provides the summary of input parameters for MIVM needed to construct ΔH_{mix} functions (**Figure 1**), in comparison with calorimetry-measured results. V_{m1} and V_{m2} were referenced to previous

thermomechanical analysis (TMA) measurements.⁷⁶ Other four parameters (Z_1 , Z_2 , B_{12} , and B_{21}) were provided by AIMD or MIVM fitting. Specifically, the RDF results of La-La, Li-K, La-Li, and La-K (**Figure 2**) were used to calculate Z_1 and Z_2 (8.76 and 8.39, respectively). In our first attempt of applying MIVM, the pair potential energies ε_{11} , ε_{22} , and ε_{12} were determined at the maximum positions of the cation-cation RDF curves (Index 1, **Figure 2**), which are also the global minima of the PMF. Using equation 2, $B_{12} = 1.11$ and $B_{21} = 1.09$ were derived and shown in **Table 2**. However, the PMF determined from this method may only include the effects of columbic interactions from separate ions in the melt which is an oversimplified approximation. The yielded “AIMD+MIVM” derived ΔH_{mix} curve (**Figure 1**) deviates more endothermically than the experimental values (also see section 2 of the SI, **Tables S2 and S5**). Recognizing such deviation originated from PMF may also attributes to the finite size effect or a sensitivity to the distribution of species in the solution sampled by AIMD, the primary reason may come from the exclusion of other effects in cation-cation PMF that are representative of non-ideal local features possibly due to the formation of complexation or oligomerization.

To take into account of the non-ideal mixing effects, we have done two kinds of modification to better connect the solvation structure to energetics. First, the PMF-related B_{ij} parameters were relaxed (with CN and molar volumes fixed) through linear regression of MIVM against experimental ΔH_{mix} values (**Figure 1**), and determined to be $B_{12} = 1.48 \pm 0.02$ and $B_{21} = 0.98 \pm 0.02$ (**Table 1**). PMF corresponding to the new B_{ij} from this “Calorimetry+MIVM” approach have values higher than those from “AIMD+MIVM”, confirming that the averaged interatomic potentials represent a solvation structure that is beyond the first cation-cation shell environment. For instance, deconvolution of the Li-K and K-Li RDFs (**Figure 2b** and **Figure S2**, respectively) reveals that the Li – K of eutectic LiCl-KCl have two coordination environments. This has likewise been observed at similar temperatures by Emerson et al.⁵¹ for the LaCl₃–NaCl molten chloride salt system, where La³⁺ was found to occupy several shallow free energy minima, with little to no barriers separating these metastable states from the global minimum.

Thus, in the second modification approach (“AIMD+Calorimetry+MIVM”), we determined PMF at the average of two deconvoluted Li-K RDF peak positions (index 1’ in **Figure 2b**) to be $\varepsilon_{22} = -3.92$ kJ/mol at 4.55 Å, in comparison to $\varepsilon_{22} = -5.85$ kJ/mol at 4.15 Å derived by the “AIMD + MIVM” approach. Similarly, the first La-Li cation-cation coordination can also be deconvoluted into two locally adjacent environments using normal distribution functions (**Figure 2c**), and yielded an averaged distance of 4.33 Å (index 1’ in **Figure 2c**). PMF of La-Li at this position was determined to be $\varepsilon_{12} = -5.47$ kJ/mol, compared to -6.04 kJ/mol at the global PMF minima (4.13 Å). These two new PMF ε_{22} and ε_{12} led to new pair-potential parameters, $B_{12} = 1.38$ and $B_{21} = 1.04$, respectively. Because their derivations were inspired by the mismatch of measured ΔH_{mix} and those reproduced by “AIMD+MIVM”, we considered them to be values still obtained

from AIMD but experimentally benchmarked. Again, applying new B_{ij} in conjunction with fixed CN and molar volumes, we can more rationally generate ΔH_{mix} based on the solvation structure.

The “AIMD+Calorimetry+MIVM” model fully reproduced ΔH_{mix} within the experimental uncertainty (**Figure 1**). The slightly endothermic character implies the MIVM model only considers binary interactions, with non-trivial corrections needed for ternary or quaternary interactions. Similar type of results was observed in the prediction of partial Gibb’s energy of the Cs – Sb – Pb alloys by Poizeau and Sadoway using the MIVM method.⁷⁷ However, unlike the aforementioned discussion, the more endothermic mixing energy predicted by MIVM was attributed to its inability to account for the first nearest neighbor interactions; whereas in our work on molten salt, missing high-order interactions is hypothesized to account for the discrepancy MIVM prediction, which will be elaborated more in the next section 3.4.

3.3 Sensitivity of MIVM to variances in input parameters

Knowing that MIVM can effectively describe and predict thermochemistry of pseudo-binary molten salt, we further examined the model sensitivity to variances of the input parameters. An iterative fitting procedure was performed through perturbations of Z_1 , Z_2 , B_{12} , and B_{21} and compared to the experimental ΔH_{mix} . This was accomplished by changing one of the parameters from **Table 1** (excluding V_{m1} and V_{m2}) by $\pm 10\%$ in magnitude while keeping all other parameters constant. The stability of model from these perturbations are presented in **Figure 3**. Perturbation in coordination number results in statistically insignificant impacts on MIVM. This also suggests that thermochemical model is relatively inert to variances in metal CN if any experimental errors present. On the other hand, it also suggests CN may not be reasonably constrained from MIVM. In contrast, variance in B_{ij} resulted in much big differences ($\sim 25\%$) in generated ΔH_{mix} from $\pm 10\%$ perturbations, suggesting a higher sensitive dependence. Accurate and rationale determination of the pair potential energies from the MIVM model is thus possible to be used with high confidence for benchmarking AIMD calculations.

Furthermore, to better distinguish the statistically significant difference between the curves produced in **Figure 3**, analysis of covariance (ANOVA)⁷⁸ was performed on the perturbed data sets (**Figure S5a**). ANOVA suggests that MIVM generated ΔH_{mix} is statistically different at the 0.05 level with data sets attained from $\pm 10\%$ perturbation of Z_2 , B_{12} , and B_{21} parameters. Additionally, ANOVA revealed that when comparing the data sets resulting from related perturbed parameters ($+Z_1$ vs. $+Z_2$, $+B_{12}$ vs. $+B_{21}$, $-Z_2$ vs. $-Z_1$ and $-B_{12}$ vs. $-B_{21}$) the distribution of the resulting values is not statistically different at the 0.05 level (**Figure 3c**). This suggests that if the paired input parameters have similar directional inaccuracies the resulting differences of MIVM fits will not be statistically distinguishable.

With the above model sensitivity analysis, we suggest that when experimental data are available the MIVM fit of measured ΔH_{mix} can be used (and perhaps the best experimental method) to constrain the pair potential energies. Reversely, the use of MIVM to extract coordination numbers should only be attempted when there is high confidence in the pair potential energies or when there is significant lack of experimental or computational inputs for the Z_1 and Z_2 parameters. This is exemplified by the calculation of impact on fit extracted from the interactive perturbation of each parameter (**Figure 3b**), which ranks B_{ij} higher importance than Z_i on perturbing ΔH_{mix} based on MIVM. This trend reiterates that the MIVM is robust to uncertainty in the coordination number of the first cation – cation shell.

3.4 Bridging ΔH_{mix} and the solvation structure of molten $\text{LaCl}_3 - \text{LiCl} - \text{KCl}$

The MIVM fit of ΔH_{mix} produced an asymmetric mixing curve with the minimum of -5.45 kJ/mol at 41.71 mol% LaCl_3 , in general agreement with previous studies of LaCl_3 mixing in alkali chlorides^{4,79}. Particularly, the magnitude of the curve and the asymmetry closely resemble those of LaCl_3 in molten NaCl ^{4,79}, likely due to the similarity of the ionic radii of Na^+ to the weighted mean of $0.58\text{Li}^+ - 0.42\text{K}^+$ cations in the eutectic.⁸⁰ The irregularity of ΔH_{mix} can be explained by the AIMD simulated solvation structure of LaCl_3 in the molten eutectic LiCl-KCl . **Figure 4** shows the solvation environment of La^{3+} at 1, 7, 20, and 100 mol% LaCl_3 , and **Figure S5** shows the CN distributions of the first shell La-Cl at corresponding LaCl_3 concentrations (**Table S8**). **Figures S3 and S4** present the evolution of RDF and CN of cation – cation and cation – anion pairs (respectively) at different LaCl_3 concentrations in the eutectic LiCl-KCl . With relevant CN and pair distances tabulated in **Tables S6 and S7** for cation-anion and cation-cation sets, respectively.

In the dilute LaCl_3 concentrations (i.e., ≤ 1 mol% LaCl_3) AIMD predicts that La^{3+} forms dominantly monomeric locally ordered structures with La primarily 6- and 7-fold coordination (67% and 32% in CN distribution, respectively) with the adjacent chlorides, forming LaCl_6^{3-} and LaCl_7^{4-} complexes. At these low concentrations, high La-Cl CN (>7) is minimal with only 1% of La coordinated by 8 Cl in the first shell (**Figure S5**). LaCl_6^{3-} has been previously hypothesized to form in alkali chloride melts,⁵⁰ with their formation further constituting the fundamental assumption of the ASM method. However, our AIMD results demonstrate that even at dilute La loadings, there is an equilibrium of the LaCl_6^{3-} and LaCl_7^{4-} complexes. A recent work by Emerson et al. also demonstrated the coexisted complexes, considering both the past and recent spectroscopic and computational studies.⁵¹

As the concentration of LaCl_3 increasing to 7 mol%, more complex solvation environments for La emerges, with the presence of LaCl_x^{y-} monomers, dimers, and trimers with approximate populations of 85.98, 11.24, and 2.78%, respectively, in the equilibrium (**Table S8**). The distribution of La-Cl CN of 6, 7,

and 8 also changes to 55, 42, and 3%, respectively, with LaCl_6^{3-} becoming less prevalent. This is likely due to the dimeric and trimeric formations within the melt which are able to stabilize La – Cl with higher coordination due to the ability of edge and corner sharing. Oligomerization continues at 20 mol%. The distribution of monomers, dimer, trimers, and oligomers ($x \geq 4$ in $\text{La}_x\text{-Cl}_x$) changes to 46.14, 14.75, 8.42 and 30.69%, respectively. At 20 mol%, the population of 7-coordinated La also increases to 45 %, comparable to that of 6-coordinated (46 %). Increasing CN and oligomerization are also previously observed in the related molten salt systems, such as $\text{LaCl}_3\text{-NaCl}$ or $\text{UCl}_3/\text{UCl}_4\text{-NaCl}$.^{51,53} Furthermore, RDF of La-Cl shows an increase of the average La-Cl CN to 6.58 at 7 mol% and 6.82 at 20 mol%, from 6.34 at 1 mol% (**Table S7**). The corresponding La-Cl distances elongate as well, by forming edge or corner sharing polyhedra to lower the polarizability induced on the shared Cl by the adjacent La, which together lead to the stabilization of the dimeric and trimeric La-Cl structures. As a result, these oligomers have higher La – Cl CN and lowered polarization of each coordinated Cl. Describing the energetic contribution of oligomers needs model beyond binary interaction. While in the MIVM method, although high-order interaction is not explicitly defined, its inclusion is a natural consequence of the “Calorimetry + MIVM” or the “AIMD + calorimetry + MIVM” approach. This is because the relaxed or benchmarked interatomic pair potential reflects an effective binary interaction that includes the mean-field effect of high-order interactions. The effective metal-metal distance (e.g., indices 1’ in **Figure 2**), based on which the averaged interatomic pair potential is defined, should always be farther than the first metal-metal coordination peak, and represents the overall oligomer geometry.

The oligomeric networks continue expanding at high LaCl_3 loading. The interconnections of the La-La are likely driven by the deficiency of chlorides provided by LiCl-KCl in the system, requiring La to form complex chloride sharing networks.¹³ At 100 mol% LaCl_3 , AIMD suggests that its molten structure can be described by salt networks of interconnected La-Cl joined by edge, corner, and face sharing polyhedra. The La – Cl CN populations are 11, 48, 34, and 7% for the 6-, 7-, 8-, and 9-coordinated environments, respectively, with an average CN of 7.37 that is in general agreement with previous studies.

The above AIMD calculated solvation structures can thus rationalize thermochemistry measured by calorimetry, with the irregular mixing behavior of ΔH_{mix} attributing to the formation of complex and concentration-dependent La-metal coordinate environments. The exothermic enthalpies of mixing can then be further explained by relaxing of induced polarization to form various oligomer salt local structures. Previous calorimetric mixing studies on LaCl_3 in alkali chloride media demonstrate that as the polarization capacity of the spacer salt cation is increased, the resulting ΔH_{mix} becomes more exothermic.²⁰ This corresponds to the ability of larger alkali cations to better “share” the Cl and allow LaCl_3 to reach its most stable thermodynamic state across the entire melt composition.⁸¹ Additionally, the larger alkali size of alkali

metals such as K, Cs, and Rb allow for greater coordination shells which enables the softer cations to stabilize the La – Cl oligomeric structures in a charge alternating network.⁸¹ Evidence of this can be observed by comparing the AIMD simulated La – Li versus La – K CN. Even though, there is more Li than K within our mixing system the RDF suggest that $CN_{La-Li} < CN_{La-K}$ at all examined $LaCl_3$ concentrations (Table S7). This may suggest that K preferentially interacts with the local chloride environment formed by the La, contributing to the non-random mixing behavior of $LaCl_3$ in LiCl-KCl. Besides polarization, the effects of Coulombic ordering and melt packing may likewise plays role in dictating the thermodynamically favored solvation state,⁸¹ which requires further studies.

4 Conclusions

In this work, for the first time, we developed a thermodynamic benchmark by using calorimetrically measured enthalpy data for interatomic potential, which are difficult to be cross-checked by other experimental techniques. The commonly employed computational methods for modeling molten salts, such as PIM and PBE-D3, fall short in accurately predicting ΔH_{mix} directly from MD trajectories. The integration of calorimetry and first-principles calculations can be realistically achieved by MIVM, enabling an effective experiment-modeling loop for complete thermodynamic understanding of salt mixing. As a showcase study for the calorimetry-model integration, we performed calorimetric experiments to determine the enthalpy mixing functions of $LaCl_3$ in eutectic LiCl-KCl across the whole La concentration range at high temperatures. AIMD was performed to generate the corresponding solvation structures, and interatomic pair potentials. Using MIVM as the platform, we found that sole use of AIMD cannot predict thermochemistry and resulted in underestimation of the exothermic nature of mixing. Calorimetry-generated ΔH_{mix} can be used to fit PMF functions and thus effectively benchmark AIMD calculations with high sensitivity. This is because MIVM is robust to errors in coordination numbers but sensitive to errors of the pair potential parameters. Furthermore, the irregular mixing behavior of ΔH_{mix} attributing to the formation of complex and concentration-dependent La-metal coordinate environments that push the effective metal-metal distance, based on which the averaged interatomic pair potential is defined, forward from the first metal-metal coordination peak. The averaged interatomic pair potential thus represents the effective binary interaction, which also potentially includes high-order interactions that are not initially included in MIVM. This study suggests a novel approach to combine experimental thermodynamics with first-principles calculations for simultaneously revealing solvation structures and energies of molten salt systems.

Acknowledgements

The authors acknowledge financial supports by the U.S. Department of Energy, Office of Nuclear Energy, Nuclear Energy University Programs via Awards No. DE-NE0009288 and DE-NE0009444. The early stage of the work was supported by Faculty Seed Grant to X.G. at Washington State University. Additional support was through collaboration, services, and infrastructure through the Nuclear Science Center User Facility at WSU, the WSU-PNNL Nuclear Science and Technology Institute, and Alexandra Navrotsky Institute for Experimental Thermodynamics. We are grateful to Rajni Chahal (ORNL) for her assistance in the setup of PIM simulations. The work at the Oak Ridge National Laboratory was supported by the Office of Materials and Chemical Technologies within the Office of Nuclear Energy, U.S. Department of Energy. This research used resources of the Oak Ridge Leadership Computing Facility, which is a DOE Office of Science User Facility, supported under Contract DE-AC05-00OR22725.

Tables

Table 1. AIMD and previously determined experimental parameters used to estimate the ΔH_{mix} of LaCl_3 in LiCl-KCl eutectic through *equation 3* (curve 1 in **Figure 1**).

Parameter	Magnitude
Z_1^\ddagger	8.76
Z_2^\ddagger	8.39*
$V_{m1}^{\dagger 76}$	70.27 cm ³ /mol
$V_{m2}^{\dagger 76}$	32.51 cm ³ /mol
B_{12}^\ddagger	1.11
B_{21}^\ddagger	1.09
B_{12}^\ddagger	1.48
B_{21}^\ddagger	0.98

‡ Obtained from AIMD in this study. *Average value. † Experimentally obtained in previous studies. ‡ Values obtained through regression fitting of experimental ΔH_{mix} by the MIVM.

Table 2. AIMD determined distances between the cation pairs with the corresponding PMF energies. PMF energies are obtained at the energetic minimum of the cation-cation pairs.

Paths	Distance (Å)	PMF (kJ/mol)
La – Cl – La ‡	5.05	-5.98
La – Cl – Li †	4.13	-6.04
La – Cl – K †	4.83	-7.36
Li – Cl – K †	4.15	-5.85
Li – Cl – K*	4.55	-3.92

‡ AIMD calculated using pure molten LaCl_3 at 1200 K, corresponding to ϵ_{11} . † AIMD calculated using pure 58mol% LiCl – 42mol% KCl eutectic at 1200 K, corresponding to ϵ_{22} . ‡ AIMD calculated using 20 mol% La loading in the LaCl_3 - LiCl-KCl system 1200 K, corresponding to ϵ_{12} components with the applied $\epsilon_{12} = 0.58(\text{La-Cl-Li}) + 0.42(\text{La-Cl-K})$ *Experimentally benchmarked ϵ_{22} pair potential.

Figures

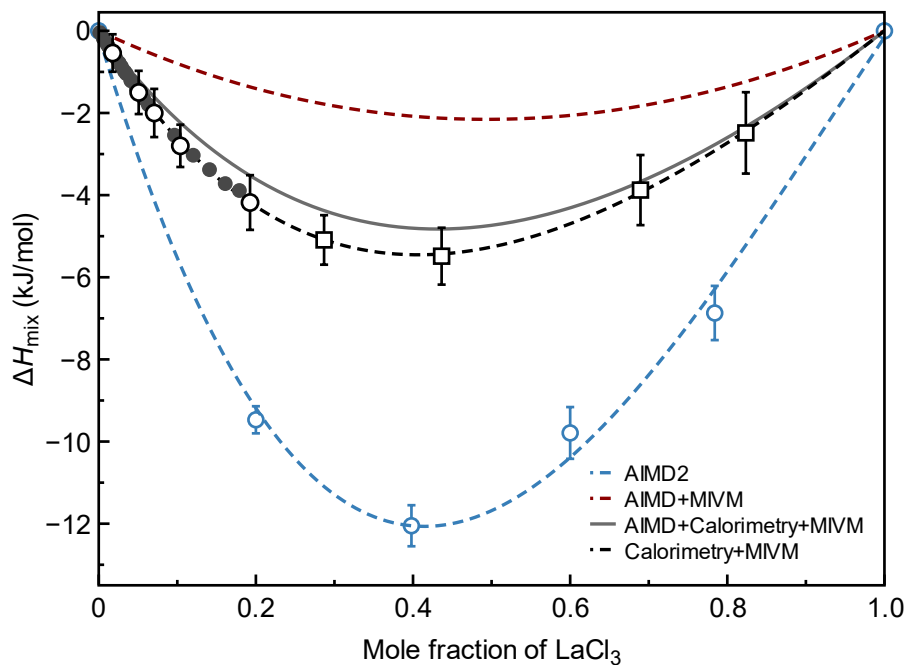


Figure 1. Experimentally and computationally obtained ΔH_{mix} in the present work. Closed and open circular data correspond to the experimental ΔH_{mix} values obtained through the continuous (ΔH_{cd}) and physical mixture drop (ΔH_{pd}) methods at 873 K; and the closed cubic data represent experimentally obtained ΔH_{mix} values through ΔH_{pd} at 1133 K. Dotted blue curve and data represent the direct computation of ΔH_{mix} from AIMD, thus labeled as AIMD2. Dotted red curve represents the ΔH_{mix} curve obtained based on inputting AIMD values to the MIVM model. Dotted black curve represents the MIVM regression fit of the experimental data with B_{12} and B_{21} as free parameters. Gray solid curve represents the ΔH_{mix} curve obtained by AIMD using MIVM and experimentally benchmarked B_{12} and B_{21} parameters.

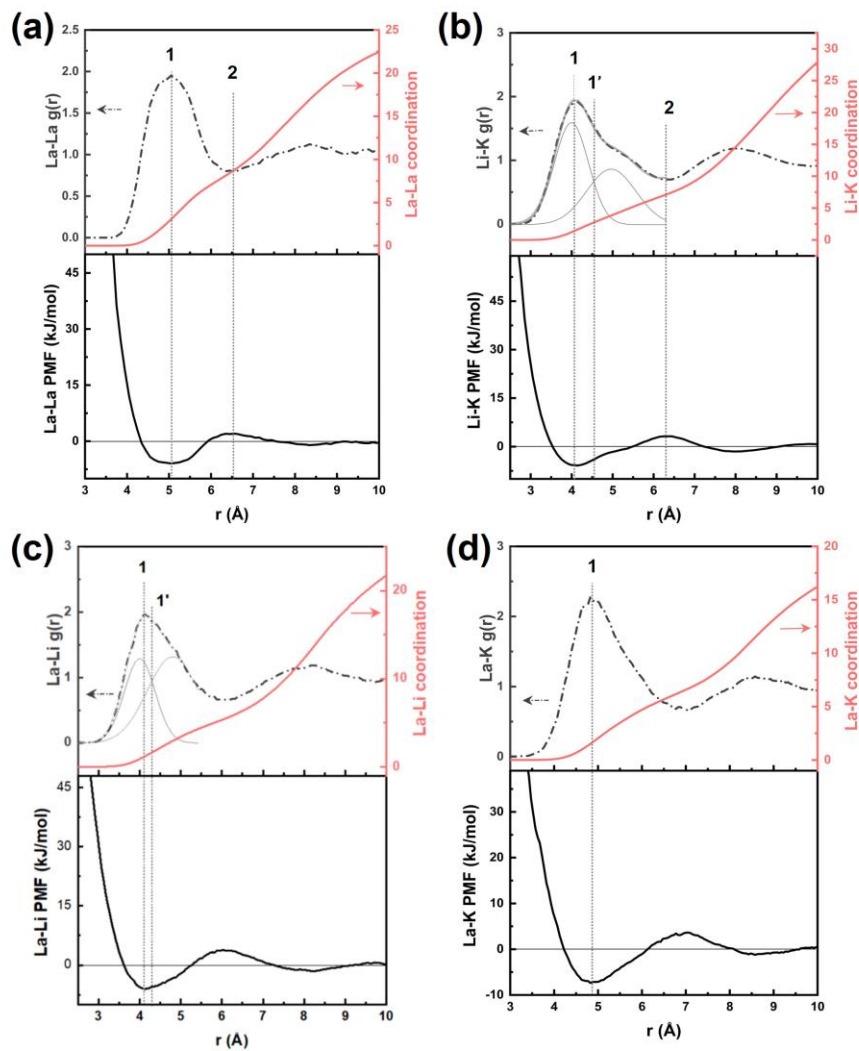


Figure 2. AIMD calculated radial distribution functions (RDF) depicted as the dashed grey curves, CN represented as solid red curves, and potentials of mean force (PMF) depicted as solid black curves, for cation-cation pairs in the $\text{LaCl}_3 - \text{LiCl-KCl}$ system. (a) La-La pairs of pure molten LaCl_3 . Dotted indexes marked by 1 and 2 represent the PMF energy for the ϵ_{11} parameter, and Z_1 La-La CN for MIVM, respectively. (b) Li-K pairs of molten 58mol% LiCl - 42mol% KCl eutectic. Dotted indexes marked by 1 and 2 represent the PMF energy for the ϵ_{22} parameter, and Z_2 Li - K CN for MIVM, respectively. Index marked by 1' corresponds to the PMF energy of the ϵ_{22} and La-Li component of ϵ_{12} parameter benchmarked by the MIVM fit of the experimental ΔH_{mix} . K-Li RDF and CN are shown in **Figure S2**. (c) La-Li pairs of molten $\text{LaCl}_3 - \text{LiCl-KCl}$ melt with 20mol% LaCl_3 loading, calculated at 873 K. Dotted index marked by 1 represents the La-Li PMF energy component for the ϵ_{12} parameter for MIVM. (d) La-K pairs of molten $\text{LaCl}_3 - \text{LiCl-KCl}$ melt at 20mol% LaCl_3 loading. Dotted index marked by 1 represents the La-K PMF energy component for the ϵ_{12} parameter for MIVM.

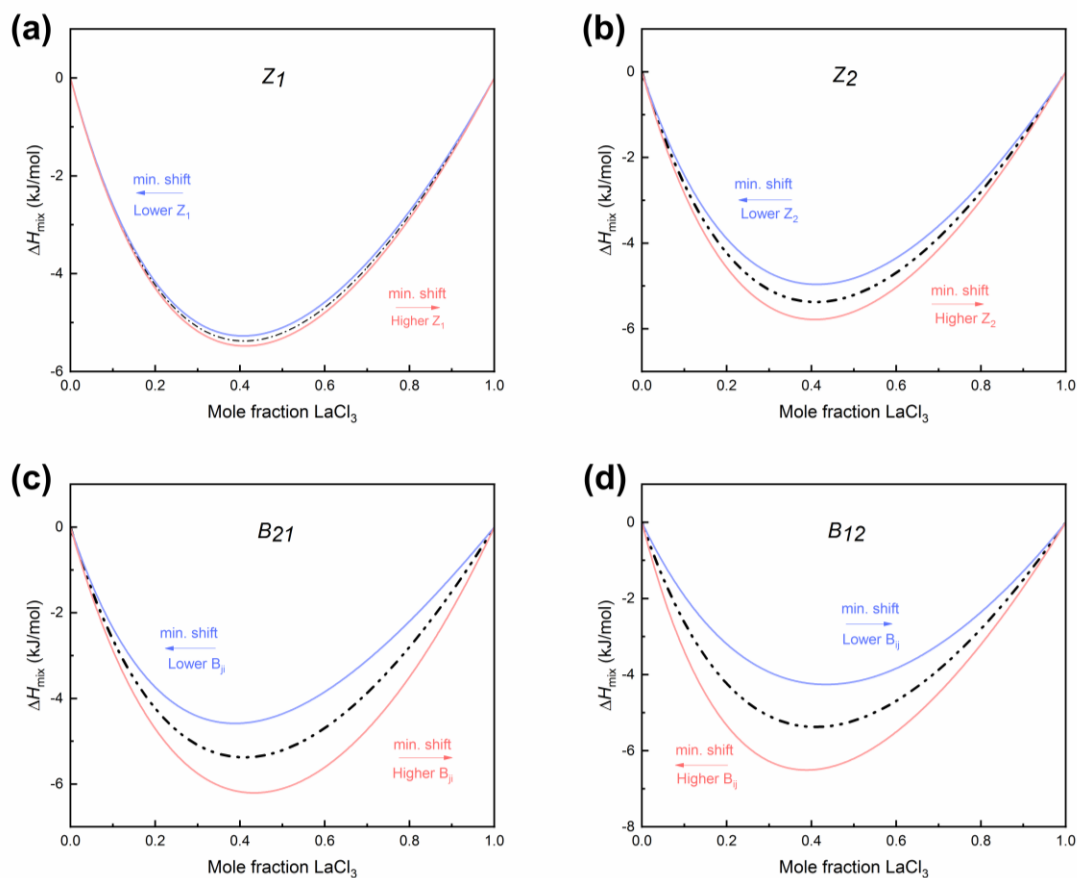


Figure 3. Iterative fitting analysis by MIVM fit of experimentally obtained ΔH_{mix} through single variable perturbation. Black dashed curve represents the MIVM fit of calorimetric data with values from **Table 1** (Z_1^\ddagger , Z_2^\ddagger , B_{12}^\ddagger and B_{21}^\ddagger). The red solid curve represents raising the magnitude of the corresponding parameter by 10% and the blue solid curve represents lowering the magnitude of the corresponding parameter by 10%. (a) Perturbation of the Z_1 parameter; (b) Perturbation of the Z_2 parameter; (c) Perturbation of the B_{21} parameter; and (d) Perturbation of the B_{12} parameter.

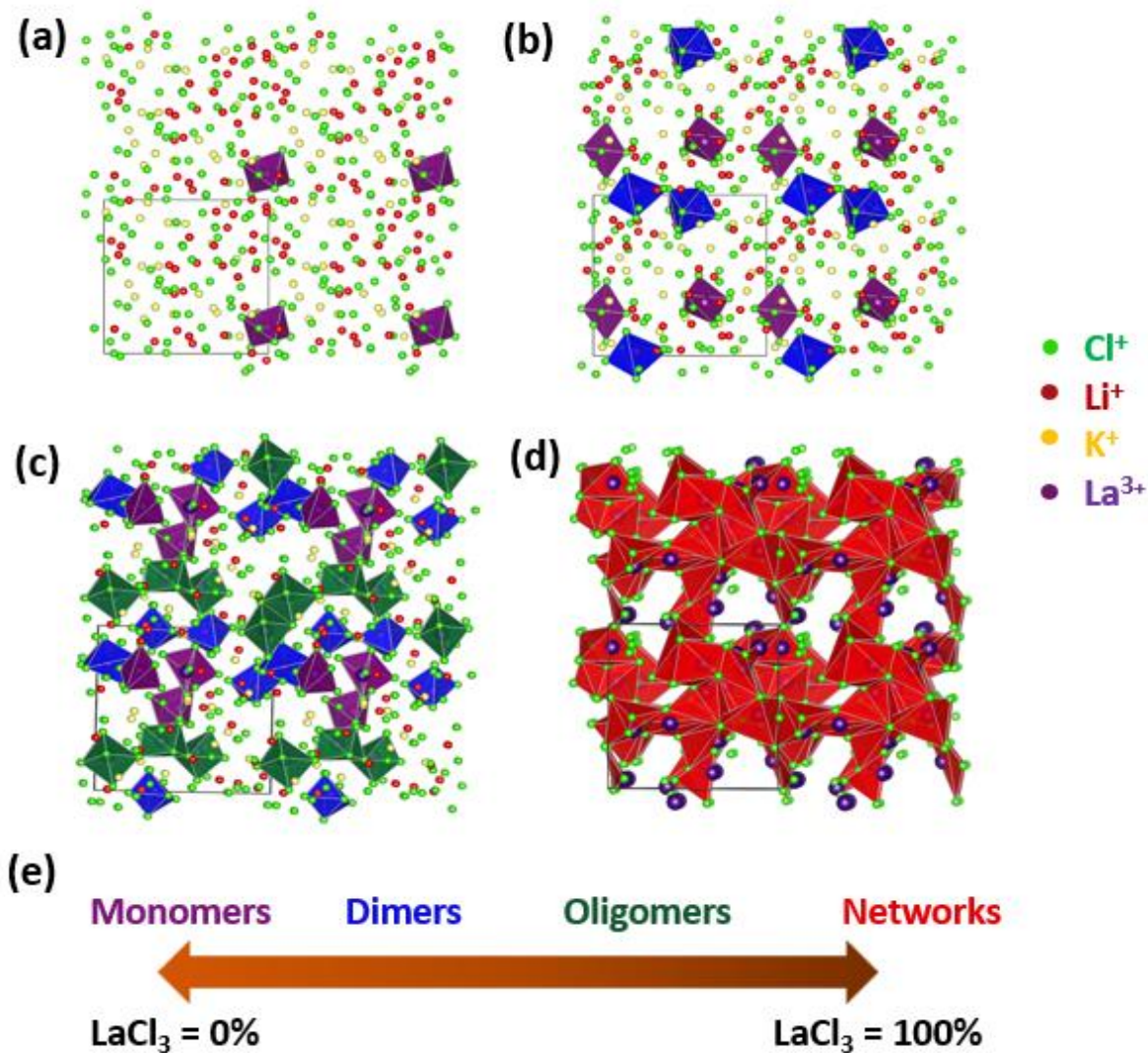


Figure 4. AIMD calculated solvation structures of LaCl_3 in 58mol% LiCl – 42mol% KCl eutectic, and the periodic boundary is outlined in black. Purple polyhedra represent the monomeric LaCl_z species (ave. $z = 6.34$), blue polyhedra dimeric the La_2Cl_z species, green polyhedra oligomer La_xCl_z ($x \geq 3$), and red polyhedra La_xCl_z networks ($x \gg 1000$). La - Cl first shell coordination distributions are demonstrated in **Figure S5** and **Table S8**. (a) LaCl_3 speciation at 1mol% LaCl_3 , calculated at 873 K;(b) LaCl_3 speciation at 7 mol% LaCl_3 , calculated at 873 K;(c) LaCl_3 speciation at 20 mol% LaCl_3 , calculated at 873 K;(d) Structure of pure LaCl_3 calculated at 1133 K; and (e) AIMD determined generalized trend of the LaCl_3 speciation in LiCl - KCl .

References

- (1) Sridharan, K.; Simpson, M. Thermal Properties of LiCl-KCl Molten Salt for Nuclear Waste Separation F I C I R&D Fuel Cycle R&D.
- (2) Novoselova, A. V.; Smolenskii, V. V. Electrochemical and Thermodynamic Properties of Lanthanides (Nd, Sm, Eu, Tm, Yb) in Alkali Metal Chloride Melts. *Radiochemistry* **2013**, *55* (3), 243–256. <https://doi.org/10.1134/S1066362213030016>.
- (3) Yin, H.; Lin, J.; Hu, B.; Liu, W.; Guo, X.; Liu, Q.; Tang, Z. Thermodynamic Description of the Constitutive Binaries of the NaCl-KCl-UCl₃-PuCl₃ System. *Calphad* **2020**, *70*, 101783. <https://doi.org/10.1016/J.CALPHAD.2020.101783>.
- (4) Schorne-Pinto, J.; Yingling, J. A.; Christian, M. S.; Mofrad, A. M.; Aslani, M. A. A.; Besmann, T. M. Correlational Approach to Predict the Enthalpy of Mixing for Chloride Melt Systems. *ACS Omega* **2022**, *7*, 362–371. <https://doi.org/10.1021/acsomega.1c04755>.
- (5) Strzelecki, A. C.; Cockreham, C. B.; Parker, S. S.; Mann, S. C.; Lhermitte, C.; Wu, D.; Guo, X.; Monreal, M.; Jackson, J. M.; Mitchell, J.; Boukhalfa, H.; Xu, H. A New Methodology for Measuring the Enthalpies of Mixing and Heat Capacities of Molten Chloride Salts Using High Temperature Drop Calorimetry. *Review of Scientific Instruments* **2024**, *95* (1). <https://doi.org/10.1063/5.0144910>.
- (6) Beneš, O.; Konings, R. J. M.; Kuenzel, C.; Sierig, M.; Dockendorf, A.; Vlahovic, L. The High-Temperature Heat Capacity of the (Li,Na)F Liquid Solution. *J Chem Thermodyn* **2009**, *41* (8), 899–903. <https://doi.org/10.1016/j.jct.2009.02.009>.
- (7) Hersh, L. S.; Kleppa, O. J. Enthalpies of Mixing in Some Binary Liquid Halide Mixtures. *J Chem Phys* **1965**, *42* (4), 1309–1322. <https://doi.org/10.1063/1.1696115>.
- (8) Rycerz, L.; Kapala, J.; Gaune-Escard, M. Experimental Mixing Enthalpy and Thermodynamic Modelling of UCl₃-KCl System. *J Mol Liq* **2021**, *342*, 116963. <https://doi.org/10.1016/j.molliq.2021.116963>.
- (9) Gaune-Escard, M.; Rycerz, L.; Bogacz, A. Enthalpies of Mixing in the DyCl₃-NaCl, DyCl₃-KCl and DyCl₃-PrCl₃ Liquid Systems. *J Alloys Compd* **1994**, *204* (1–2), 185–188. [https://doi.org/10.1016/0925-8388\(94\)90089-2](https://doi.org/10.1016/0925-8388(94)90089-2).
- (10) Chojnacka, I.; Rycerz, L.; Kapala, J.; Gaune-Escard, M. Calorimetric Investigation of TmCl₃-MCl Liquid Mixtures (M = Li, Na, K, Rb). *J Mol Liq* **2020**, *319*, 113935. <https://doi.org/10.1016/j.molliq.2020.113935>.
- (11) Kleppa, O. J.; Hong, K. C. Enthalpies of Mixing in Liquid Alkaline Earth Fluoride-Alkali Fluoride Mixtures. II. Calcium Fluoride with Lithium, Sodium, and Potassium Fluorides. *J Phys Chem* **1974**, *78* (15), 1478–1481. <https://doi.org/10.1021/j100608a007>.
- (12) Hong, K. C.; Kleppa, O. J. Thermochemistry of Binary Liquid Mixtures of Alkali Fluorides with Lanthanide Trifluorides. *J Phys Chem* **1979**, *83* (20), 2589–2593. <https://doi.org/10.1021/j100483a008>.

- (13) Feng, T.; Zhao, J.; Liang, W.; Lu, G. Molecular Dynamics Simulations of Lanthanum Chloride by Deep Learning Potential. *Comput Mater Sci* **2022**, *210*, 111014. <https://doi.org/10.1016/j.commatsci.2021.111014>.
- (14) Andersson, D. A.; Beeler, B. W. Ab Initio Molecular Dynamics (AIMD) Simulations of NaCl, UCl₃ and NaCl-UCl₃ Molten Salts. *Journal of Nuclear Materials* **2022**, *568*, 153836. <https://doi.org/10.1016/j.jnucmat.2022.153836>.
- (15) Andersson, D. A.; Wang, G.; Yang, P.; Beeler, B. W. KCl-UCl₃ Molten Salts Investigated by Ab Initio Molecular Dynamics (AIMD) Simulations: A Comparative Study with Three Dispersion Models. *Journal of Nuclear Materials* **2024**, *599*, 155226. <https://doi.org/10.1016/j.jnucmat.2024.155226>.
- (16) Duemmler, K.; Andersson, D.; Beeler, B. First-Principles Investigation of the Thermophysical Properties of NaCl, PuCl₃, and NaCl-PuCl₃ Molten Salts. *Journal of Nuclear Materials* **2024**, *591*, 154902. <https://doi.org/10.1016/j.jnucmat.2024.154902>.
- (17) Roy, S.; Liu, Y.; Topsakal, M.; Dias, E.; Gakhar, R.; Phillips, W. C.; Wishart, J. F.; Leshchev, D.; Halstenberg, P.; Dai, S.; Gill, S. K.; Frenkel, A. I.; Bryantsev, V. S. A Holistic Approach for Elucidating Local Structure, Dynamics, and Speciation in Molten Salts with High Structural Disorder. *J Am Chem Soc* **2021**, *143* (37), 15298–15308. <https://doi.org/10.1021/jacs.1c06742>.
- (18) Li, B.; Dai, S.; Jiang, D. First-Principles Molecular Dynamics Simulations of UCl_n-NaCl (n = 3, 4) Molten Salts. *ACS Appl Energy Mater* **2019**, *2* (3), 2122–2128. <https://doi.org/10.1021/acsaem.8b02157>.
- (19) Spencer, P. J. A Brief History of CALPHAD. *Calphad* **2008**, *32* (1), 1–8. <https://doi.org/10.1016/J.CALPHAD.2007.10.001>.
- (20) Schorne-Pinto, J.; Yingling, J. A.; Christian, M. S.; Mofrad, A. M.; Aslani, M. A. A.; Besmann, T. M. Correlational Approach to Predict the Enthalpy of Mixing for Chloride Melt Systems. *ACS Omega* **2022**, *7* (1), 362–371. <https://doi.org/10.1021/acsomega.1c04755>.
- (21) Tao, D. P. Correct Expressions of Enthalpy of Mixing and Excess Entropy from MIVM and Their Simplified Forms. *Metallurgical and Materials Transactions B: Process Metallurgy and Materials Processing Science* **2016**, *47* (1), 1–9. <https://doi.org/10.1007/S11663-015-0460-5/TABLES/3>.
- (22) Dong Ping Tao. A New Model of Thermodynamics of Liquid Mixtures and Its Application to Liquid Alloys. *Thermochim Acta* **2000**, *363* (1–2), 105–113. [https://doi.org/10.1016/S0040-6031\(00\)00603-1](https://doi.org/10.1016/S0040-6031(00)00603-1).
- (23) HUTCHINSON, F.; WILSON, M.; MADDEN, P. A. A Unified Description of MCl₃ Systems with a Polarizable Ion Simulation Model. *Mol Phys* **2001**, *99* (10), 811–824. <https://doi.org/10.1080/00268970010022878>.
- (24) Salanne, M.; Simon, C.; Turq, P.; Madden, P. A. Calculation of Activities of Ions in Molten Salts with Potential Application to the Pyroprocessing of Nuclear Waste. *J Phys Chem B* **2008**, *112* (4), 1177–1183. <https://doi.org/10.1021/jp075299n>.

- (25) Okamoto, Y.; Suzuki, S.; Shiwaku, H.; Ikeda-Ohno, A.; Yaita, T.; Madden, P. A. Local Coordination about La^{3+} in Molten LaCl_3 and Its Mixtures with Alkali Chlorides. *J Phys Chem A* **2010**, *114* (13), 4664–4671. <https://doi.org/10.1021/jp910637p>.
- (26) Fredrickson, G. L.; Patterson, M. N.; Vaden, D. E.; Galbreth, G. G.; Yoo, T. S.; Price, J. C.; Flynn, E. J.; Searle, R. N. History and Status of Spent Fuel Treatment at the INL Fuel Conditioning Facility. *Progress in Nuclear Energy* **2022**, *143*, 104037. <https://doi.org/10.1016/J.PNUCENE.2021.104037>.
- (27) Sridharan, K.; Allen, T.; Anderson, M.; Simpson, M. Thermal Properties of LiCl-KCl Molten Salt for Nuclear Waste Separation. **2012**. <https://doi.org/10.2172/1058922>.
- (28) Choppin, G. R.; Wong, P. J. Current Status of Radioactive Waste Disposal. *J Radioanal Nucl Chem* **1996**, *203* (2), 575–590. <https://doi.org/10.1007/BF02041530/METRICS>.
- (29) Rodríguez-Penalonga, L.; Yolanda Moratilla Soria, B. A Review of the Nuclear Fuel Cycle Strategies and the Spent Nuclear Fuel Management Technologies. *Energies* **2017**, *Vol. 10*, Page 1235 **2017**, *10* (8), 1235. <https://doi.org/10.3390/EN10081235>.
- (30) Bruno, J.; Ewing, R. C. Spent Nuclear Fuel. *Elements* **2006**, *2* (6), 343–349. <https://doi.org/10.2113/GSELEMENTS.2.6.343>.
- (31) MIT. MIT Study on the Future of Nuclear Fuel Cycle. *The Future of the Nuclear Fuel Cycle* **2010**, 43–53.
- (32) *Spent Nuclear Fuel Reprocessing Flowsheet*. https://inis.iaea.org/collection/NCLCollectionStore/_Public/47/093/47093761.pdf (accessed 2023-01-16).
- (33) Simpson, M. F. Developments of Spent Nuclear Fuel Pyroprocessing Technology at Idaho National Laboratory. **2012**. <https://doi.org/10.2172/1044209>.
- (34) Choi, E. Y.; Jeong, S. M. Electrochemical Processing of Spent Nuclear Fuels: An Overview of Oxide Reduction in Pyroprocessing Technology. *Progress in Natural Science: Materials International* **2015**, *25* (6), 572–582. <https://doi.org/10.1016/J.PNSC.2015.11.001>.
- (35) Nawada, H. P.; Fukuda, K. Role of Pyro-Chemical Processes in Advanced Fuel Cycles. *Journal of Physics and Chemistry of Solids* **2005**, *66* (2–4), 647–651. <https://doi.org/10.1016/J.JPCS.2004.07.022>.
- (36) Migdisov, A.; Guo, X.; Nisbet, H.; Xu, H.; Williams-Jones, A. E. Fractionation of REE, U, and Th in Natural Ore-Forming Hydrothermal Systems: Thermodynamic Modeling. *Journal of Chemical Thermodynamics* **2019**, *128*. <https://doi.org/10.1016/j.jct.2018.08.032>.
- (37) Hur, J. M.; Kim, T. J.; Choi, I. K.; Do, J. B.; Hong, S. S.; Seo, C. S. Chemical Behavior of Fission Products in the Pyrochemical Process. *Nucl Technol* **2017**, *162* (2), 192–198. <https://doi.org/10.13182/NT08-A3947>.
- (38) Ackerman, J. P. Chemical Basis for Pyrochemical Reprocessing of Nuclear Fuel. *Ind. Eng. Chem. Res.* **1991**, *30* (1), 141–145.

- (39) CHO, Y.-Z.; PARK, G.-H.; YANG, H.-C.; HAN, D.-S.; LEE, H.-S.; KIM, I.-T. Minimization of Eutectic Salt Waste from Pyroprocessing by Oxidative Precipitation of Lanthanides. *J Nucl Sci Technol* **2009**, *46* (10), 1004–1011. <https://doi.org/10.1080/18811248.2009.9711610>.
- (40) Glatz, J. P.; Malmbeck S. R. *Reprocessing and Recycling of Spent Nuclear Fuel*; Taylor, R., Ed.; 2015.
- (41) Naumov, V. S.; Bychkov, A. V; Lebedev, V. A. *Mixing Enthalpy of TbCl₃-MCl Liquid Mixtures (M = Li, Na, K, Rb, Cs)*; GauneEscard, M., Ed.; Begell House, 1999.
- (42) Dienstbach, F.; Blachnik, R. Mischungsenthalpien von Geschmolzenen Alkalihalogenid-Lanthanoidenhalogenidsystemen. *Z Anorg Allg Chem* **1975**, *412* (2), 97–109. <https://doi.org/10.1002/ZAAC.19754120202>.
- (43) Gaune-Escard, M.; Bogacz, A.; Rycerz, L.; Szczepaniak, W. Calorimetric Investigation of NdCl₃-MCl Liquid Mixtures (Where M Is Na, K, Rb, Cs). *Thermochim Acta* **1994**, *236* (C), 67–80. [https://doi.org/10.1016/0040-6031\(94\)80256-4](https://doi.org/10.1016/0040-6031(94)80256-4).
- (44) Chojnacka, I.; Rycerz, L.; Kapala, J.; Gaune-Escard, M. Calorimetric Investigation of TmCl₃-MCl Liquid Mixtures (M = Li, Na, K, Rb). *J Mol Liq* **2020**, *319*, 113935. <https://doi.org/10.1016/J.MOLLIQ.2020.113935>.
- (45) Papatheodorou, G. N.; Kleppa, O. J. Thermodynamic Studies of Binary Charge Unsymmetrical Fused Salt Systems. Cerium(III) Chloride-Alkali Chloride Mixtures. *Journal of Physical Chemistry* **1974**, *78* (2), 178–181. https://doi.org/10.1021/J100595A018/SUPPL_FILE/J100595A018_SI_001.PDF.
- (46) Papatheodorou, G. N.; Østvold, T. Thermodynamic Studies of Binary Charge Unsymmetrical Fused Salt Systems. Calorimetric and Electromotive Force Measurements of Liquid Lanthanum(III) Chloride-Alkali Chloride Mixtures. *Journal of Physical Chemistry* **1974**, *78* (2), 181–185. https://doi.org/10.1021/J100595A019/SUPPL_FILE/J100595A019_SI_001.PDF.
- (47) Papatheodorou, G. N.; Waernes, O.; Krantz, A. Thermodynamic Studies of Binary Charged Unsymmetrical Fused Salt Systems. Calorimetric and Electromotive Force Measurements of Yttrium(III) Chloride-Alkali. *Aca Chemica Scandinavica A* **1979**, *33*. <https://doi.org/10.3891/acta.chem.scand.33a-0173>.
- (48) Winner, N.; Williams, H.; Scarlat, R. O.; Asta, M. Ab-Initio Simulation Studies of Chromium Solvation in Molten Fluoride Salts. *J Mol Liq* **2021**, *335*, 116351. <https://doi.org/10.1016/j.molliq.2021.116351>.
- (49) Feng, T.; Zhao, J.; Liang, W.; Lu, G. Molecular Dynamics Simulations of Lanthanum Chloride by Deep Learning Potential. *Comput Mater Sci* **2022**, *210*, 111014. <https://doi.org/10.1016/j.commatsci.2021.111014>.
- (50) Papatheodorou, G. N.; Ostvold, T. Thermodynamic Studies of Binary Charge Unsymmetrical Fused Salt Systems. Calorimetric and Electromotive Force Measurements of Liquid Lanthanum(III) Chloride-Alkali Chloride Mixtures. *J Phys Chem* **1974**, *78* (2), 181–185. <https://doi.org/10.1021/j100595a019>.

- (51) Emerson, M. S.; Sharma, S.; Roy, S.; Bryantsev, V. S.; Ivanov, A. S.; Gakhar, R.; Woods, M. E.; Gallington, L. C.; Dai, S.; Maltsev, D. S.; Margulis, C. J. Complete Description of the LaCl_3 – NaCl Melt Structure and the Concept of a Spacer Salt That Causes Structural Heterogeneity. *J Am Chem Soc* **2022**, *144* (47), 21751–21762. <https://doi.org/10.1021/jacs.2c09987>.
- (52) Hatem, G. Semi-Emperical Dependence of the Excess Functions of Asymmetrical Molten Salt Systems. *Thermochim Acta* **1999**, *338* (1–2), 95–102. [https://doi.org/10.1016/S0040-6031\(99\)00194-X](https://doi.org/10.1016/S0040-6031(99)00194-X).
- (53) Li, B.; Dai, S.; Jiang, D. First-Principles Molecular Dynamics Simulations of UCl_n – NaCl ($n = 3, 4$) Molten Salts. *ACS Appl Energy Mater* **2019**, *2* (3), 2122–2128. <https://doi.org/10.1021/acsaem.8b02157>.
- (54) Smith, A. L.; Capelli, E.; Konings, R. J. M.; Gheribi, A. E. A New Approach for Coupled Modelling of the Structural and Thermo-Physical Properties of Molten Salts. Case of a Polymeric Liquid LiF – BeF_2 . *J Mol Liq* **2020**, *299*, 112165. <https://doi.org/10.1016/j.molliq.2019.112165>.
- (55) van Oudenaren, G. I. L.; Ocadiz-Flores, J. A.; Smith, A. L. Coupled Structural-Thermodynamic Modelling of the Molten Salt System NaCl – UCl_3 . *J Mol Liq* **2021**, *342*, 117470. <https://doi.org/10.1016/j.molliq.2021.117470>.
- (56) Schreuder, M. B. J. W.; Ocadiz Flores, J. A.; Gheribi, A. E.; Beneš, O.; Griveau, J.-C.; Colineau, E.; Konings, R. J. M.; Smith, A. L. Experimental and Computational Exploration of the NaF – ThF_4 Fuel System: Structure and Thermochemistry. *J Phys Chem B* **2021**, *125* (30), 8558–8571. <https://doi.org/10.1021/acs.jpccb.1c04830>.
- (57) Poizeau, S.; Sadoway, D. R. Application of the Molecular Interaction Volume Model (MIVM) to Calcium-Based Liquid Alloys of Systems Forming High-Melting Intermetallics. *J. Am. Chem. Soc* **2013**, *135*, 44. <https://doi.org/10.1021/ja4013886>.
- (58) Tao, D. P.; Li, D. F.; Yang, B. Prediction of the Thermodynamic Properties of Quaternary Liquid Alloys by Modified Coordination Equation. *Thermochim Acta* **2002**, *383* (1–2), 45–51. [https://doi.org/10.1016/S0040-6031\(01\)00655-4](https://doi.org/10.1016/S0040-6031(01)00655-4).
- (59) Guo, X.; Boukhalfa, H.; Mitchell, J. N.; Ramos, M.; Gaunt, A. J.; Migliori, A.; Roback, R. C.; Navrotsky, A.; Xu, H. Sample Seal-and-Drop Device and Methodology for High Temperature Oxide Melt Solution Calorimetric Measurements of PuO_2 . *Review of Scientific Instruments* **2019**, *90* (4), 044101. <https://doi.org/10.1063/1.5093567>.
- (60) Guo, X.; Boukhalfa, H.; Mitchell, J. N.; Ramos, M.; Gaunt, A. J.; Migliori, A.; Roback, R. C.; Navrotsky, A.; Xu, H. Sample Seal-and-Drop Device and Methodology for High Temperature Oxide Melt Solution Calorimetric Measurements of PuO_2 . *Review of Scientific Instruments* **2019**, *90* (4). <https://doi.org/10.1063/1.5093567>.
- (61) Strzelecki, A. C.; Cockreham, C. B.; Parker, S. S.; Mann, S. C.; Lhermitte, C.; Wu, D.; Guo, X.; Monreal, M.; Jackson, J. M.; Mitchell, J.; Boukhalfa, H.; Xu, H. A New Methodology for Measuring the Enthalpies of Mixing and Heat Capacities of Molten Chloride Salts Using High Temperature Drop Calorimetry. *Review of Scientific Instruments* **2024**, *95* (1). <https://doi.org/10.1063/5.0144910>.

- (62) Lonergan, J.; Goncharov, V.; Swinhart, M.; Makovsky, K.; Rollog, M.; McNamara, B.; Clark, R.; Cutforth, D.; Armstrong, C.; Guo, X.; Paviet, P. Thermodynamic Investigation of the NaCl-KCl Salt System from 25 to 950 °C. *J Mol Liq* **2023**, *391*, 122591. <https://doi.org/10.1016/j.molliq.2023.122591>.
- (63) Kühne, T. D.; Iannuzzi, M.; Del Ben, M.; Rybkin, V. V.; Seewald, P.; Stein, F.; Laino, T.; Khaliullin, R. Z.; Schütt, O.; Schiffmann, F.; Golze, D.; Wilhelm, J.; Chulkov, S.; Bani-Hashemian, M. H.; Weber, V.; Borštnik, U.; Taillefumier, M.; Jakobovits, A. S.; Lazzaro, A.; Pabst, H.; Müller, T.; Schade, R.; Guidon, M.; Andermatt, S.; Holmberg, N.; Schenter, G. K.; Hehn, A.; Bussy, A.; Belleflamme, F.; Tabacchi, G.; Glöß, A.; Lass, M.; Bethune, I.; Mundy, C. J.; Plessl, C.; Watkins, M.; VandeVondele, J.; Krack, M.; Hutter, J. CP2K: An Electronic Structure and Molecular Dynamics Software Package - Quickstep: Efficient and Accurate Electronic Structure Calculations. *J Chem Phys* **2020**, *152* (19). <https://doi.org/10.1063/5.0007045>.
- (64) VandeVondele, J.; Krack, M.; Mohamed, F.; Parrinello, M.; Chassaing, T.; Hutter, J. Quickstep: Fast and Accurate Density Functional Calculations Using a Mixed Gaussian and Plane Waves Approach. *Comput Phys Commun* **2005**, *167* (2), 103–128. <https://doi.org/10.1016/j.cpc.2004.12.014>.
- (65) Janz, G. J.; Tomkins, R. P. T.; Allen, C. B.; Downey, J. R.; Garner, G. L.; Krebs, U.; Singer, S. K. Molten Salts: Volume 4, Part 2, Chlorides and Mixtures—Electrical Conductance, Density, Viscosity, and Surface Tension Data. *J Phys Chem Ref Data* **1975**, *4* (4), 871–1178. <https://doi.org/10.1063/1.555527>.
- (66) Mariani, R. D.; Vaden, D. Modeled Salt Density for Nuclear Material Estimation in the Treatment of Spent Nuclear Fuel. *Journal of Nuclear Materials* **2010**, *404* (1), 25–32. <https://doi.org/10.1016/j.jnucmat.2010.06.022>.
- (67) Martínez, L.; Andrade, R.; Birgin, E. G.; Martínez, J. M. P. <sc>ACKMOL</Sc> : A Package for Building Initial Configurations for Molecular Dynamics Simulations. *J Comput Chem* **2009**, *30* (13), 2157–2164. <https://doi.org/10.1002/jcc.21224>.
- (68) Basin, A. S.; Kaplun, A. B.; Meshalkin, A. B.; Uvarov, N. F. The LiCl-KCl Binary System. *Russian Journal of Inorganic Chemistry* **2008**, *53* (9), 1509–1511. <https://doi.org/10.1134/S003602360809026X>.
- (69) Lu, J.-B.; Cantu, D. C.; Nguyen, M.-T.; Li, J.; Glezakou, V.-A.; Rousseau, R. Norm-Conserving Pseudopotentials and Basis Sets To Explore Lanthanide Chemistry in Complex Environments. *J Chem Theory Comput* **2019**, *15* (11), 5987–5997. <https://doi.org/10.1021/acs.jctc.9b00553>.
- (70) VandeVondele, J.; Hutter, J. Gaussian Basis Sets for Accurate Calculations on Molecular Systems in Gas and Condensed Phases. *J Chem Phys* **2007**, *127* (11). <https://doi.org/10.1063/1.2770708>.
- (71) Grimme, S.; Antony, J.; Ehrlich, S.; Krieg, H. A Consistent and Accurate *Ab Initio* Parametrization of Density Functional Dispersion Correction (DFT-D) for the 94 Elements H-Pu. *J Chem Phys* **2010**, *132* (15). <https://doi.org/10.1063/1.3382344>.
- (72) Perdew, J. P.; Burke, K.; Ernzerhof, M. Generalized Gradient Approximation Made Simple. *Phys Rev Lett* **1996**, *77* (18), 3865–3868. <https://doi.org/10.1103/PhysRevLett.77.3865>.

- (73) Goedecker, S.; Teter, M.; Hutter, J. Separable Dual-Space Gaussian Pseudopotentials. *Phys Rev B* **1996**, *54* (3), 1703–1710. <https://doi.org/10.1103/PhysRevB.54.1703>.
- (74) Rohrbach, A.; Hafner, J.; Kresse, G. Electronic Correlation Effects in Transition-Metal Sulfides. *Journal of Physics: Condensed Matter* **2003**, *15* (6), 979–996. <https://doi.org/10.1088/0953-8984/15/6/325>.
- (75) Chapleski, R. C.; Ivanov, A. S.; Peterson, K. A.; Bryantsev, V. S. Improving the Theoretical Description of Ln(III)/An(III) Separation with Phosphinic Acid Ligands: A Benchmarking Study of Structure and Selectivity. *Physical Chemistry Chemical Physics* **2021**, *23* (35), 19558–19570. <https://doi.org/10.1039/D1CP02466C>.
- (76) Zhang, C.; Simpson, M. F. Density of Molten Salt Mixtures of Eutectic LiCl-KCl Containing UCl₃, CeCl₃, or LaCl₃. *Journal of Nuclear Fuel Cycle and Waste Technology(JNFCWT)* **2017**, *15* (2), 117–124. <https://doi.org/10.7733/JNFCWT.2017.15.2.117>.
- (77) Poizeau, S.; Sadoway, D. R. Application of the Molecular Interaction Volume Model (MIVM) to Calcium-Based Liquid Alloys of Systems Forming High-Melting Intermetallics. *J Am Chem Soc* **2013**, *135* (22), 8260–8265. <https://doi.org/10.1021/ja4013886>.
- (78) Breitsohl, H. Beyond ANOVA: An Introduction to Structural Equation Models for Experimental Designs. *Organ Res Methods* **2019**, *22* (3), 649–677. https://doi.org/10.1177/1094428118754988/ASSET/IMAGES/LARGE/10.1177_1094428118754988-FIG2.JPEG.
- (79) Papatheodorou, G. N.; Østvold, T. Thermodynamic Studies of Binary Charge Unsymmetrical Fused Salt Systems. Calorimetric and Electromotive Force Measurements of Liquid Lanthanum(III) Chloride-Alkali Chloride Mixtures. *Journal of Physical Chemistry* **1974**, *78* (2), 181–185. https://doi.org/10.1021/J100595A019/SUPPL_FILE/J100595A019_SI_001.PDF.
- (80) *Database of Ionic Radii*. <http://abulafia.mt.ic.ac.uk/shannon/> (accessed 2023-01-16).
- (81) Adya, A. K. Structural and Thermodynamic Properties of Molten UCl₃ and UCl₃-MCl (M = Li, Na, K, and Cs) Systems. *ECS Proceedings Volumes* **1999**, *1999-41* (1), 341–355. <https://doi.org/10.1149/199941.0341PV>.